International Journal of Image Processing and Vision Science

Volume 2 | Issue 3 Article 3

May 2022

Nonlinear Spectral Unmixing using Semi-Supervised Standard Fuzzy Clustering

Shaheera Rashwan
IRI, City of SRTA, Alexandria, Egypt, rashwan.shaheera@gmail.com

Recommended Citation

Rashwan, Shaheera (2022) "Nonlinear Spectral Unmixing using Semi-Supervised Standard Fuzzy Clustering," *International Journal of Image Processing and Vision Science*: Vol. 2: Iss. 3, Article 3.
DOI: 10.47893/IJIPVS.2022.1084
Available at: https://www.interscience.in/ijipvs/vol2/iss3/3

Nonlinear Spectral Unmixing using Semi-Supervised Standard Fuzzy Clustering

Shaheera Rashwan
Informatics Research Institute, City of Scientific Research and Technological Applications, New Borg Elarab, Alexandria, Egypt
srashwan@srtacity.sci.eg

Abstract:

Coarse resolution captured in remote sensing causes the combination of different materials in one pixel, called the mixed pixel. Spectral unmixing estimates the combination of endmembers in mixed pixels and their corresponding abundance maps in the Hyper/Multi spectral image. In this paper, a nonlinear spectral unmixing based on semi-supervised fuzzy clusteringis proposed. First, pure pixels (endmembers) using Vertex Component Analysis (VCA) are extracted and those pixels are the labelled pixels where the membership value of each is 1 for the corresponding endmember and 0 for the others. Second, the semi-supervised fuzzy clustering is appliedto find the membership matrix defining the fraction of the endmember in each mixed pixel and hence extract the abundance maps. The experiments were conducted on both synthetic data such as the Legendre data and real data such as Jasper Ridge data. The non-linearity of the Legendre data was performed by the Fan model on different signal-to-noise ratio values. The results of the new unmixing model show its significant performance when compared with four state-of the art unmixing algorithms.

Keywords: Nonlinear Unmixing, Fuzzy Clustering, Abundance Maps

1. Introduction

The reflectance of a pixel in remote sensing images is a combination of the pure spectral signatures of materials which exist in the captured area. Spectral unmixing (SU) is the extraction of the pure element spectral signatures and their proportions for each pixel. The simplest form of mixing models is the linear mixing model (LMM) which combines the observed reflectance vectors into a convex hull of the pure spectral signatures, named endmembers. The LMM is effective in scenes where the materials cover a large area according to the pixel size [1]. However, nonlinear interactions between materials happen in many scenes where there is complex radiation occurring by different endmembers [2]. In those situations, nonlinear mixing models should be considered [1], [3].

Different clustering methods [4-7] have been used in nonlinear spectral unmixing, among which fuzzy based techniques are widely used. In hard clustering (i.e. k-means) the membership of a single pixel is corresponding to only one cluster while fuzzy based techniques give the chance to be corresponding to multiple clusters based on the partial membership for a single pixel [8-11].

In the conventional fuzzy c-means [4, 12], the spectral unmixing of the hyperspectral pixels performed better if the degree of uncertainty of the neighboring region is small and the

image is free of noise. For this reason, various versions of fuzzy based clustering techniques have been developed to add the spatial information to overcome the effect of noise [10, 13-15]. The spatial information was incorporated in the FCM (FCM-S) [8] to tackle the problem of the spatial non-homogeneity and allow the pixel to get affected by its neighbours, but the effect of noise cannot be recovered totally. To handle this issue, a fuzzy local information c-means (FLICM), was proposed by Krinidis and Chatzis [10] and the objective function of the conventional FCM has also been improved by introducing a clustering entropy to the objective function as well [16].

All the above versions of Fuzzy c-means methods are unsupervised clustering methods and have been widely used in spectral unmixing [17-21]. However, the pure pixels can be identified easily and accurately using one of the endmember extraction algorithms such as pixel purity index (PPI) [22], vertex component analysis (VCA) [23], etc… and pure pixels have definitely membership 1 for the corresponding endmember and memberships 0 for the remaining endmembers. Based on the priori knowledge of pure pixels' memberships, a new nonlinear spectral unmixing has been developed in this paper using a semi supervised version of the fuzzy c-means [24] to get a strong initialization of the clusters in order to discard the pixel noise and increase the accuracy of the unmixing model.

2. Methodology

2.1 Background

The main aim in this work is how to construct the classification of n numbers of data:

$$X = \{x_k | x_k = (x_{k1}, \dots, x_{kp})^T \in R^p, k = 1, \dots, n\} \quad (1)$$

Into c numbers of clusters which are represented as cluster centers:

$$V = \{v_i | v_i = (v_{i1}, \dots, v_{ip})^T \in R^p, i = 1, \dots, c\} \quad (2)$$

The Euclidean norm is computed on the space R^p by:

$$\|x_k - v_i\| = \sqrt{\sum_{j=1}^{p} (x_{kj} - v_{ij})^2} \quad (3)$$

Now, the membership grade that x_k belongs to a cluster i is $u_{ki} \in [0,1]$ and the goal of the classification is to get the matrix U for all data and all clusters where $\sum_{i=1}^{c} u_{ki} = 1$. Consequently, the supervised degree of membership that x_k belongs to a cluster i is $\bar{u}_{ki} \in [0,1]$ which is given initially for certain x_k and cluster i and in case it is not given, its value is 0. Hence, the equation $\sum_{i=1}^{c} \bar{u}_{ki} \leq 1$ represents the conditions in $\bar{U}$

The optimal solution v_i is given by

$$v_i = \frac{\sum_{k=1}^{n} |u_{ki} - \bar{u}_{ki}|^m x_k}{\sum_{k=1}^{n} |u_{ki} - \bar{u}_{ki}|^m} \quad (4)$$

Where

$$u_{ki} = \bar{u}_{ki} + \left(1 - \sum_{j=1}^{c} \bar{u}_{kj}\right) \frac{\left(\frac{1}{d_{ki}}\right)^{\frac{1}{m-1}}}{\sum_{j=1}^{c}\left(\frac{1}{d_{kj}}\right)^{\frac{1}{m-1}}} \quad (5)$$

Such that:

$$d_{ki} = \|x_k - v_i\|^2 \quad (6)$$

To be noted that

$$1 - \sum_{j=1}^{c} \bar{u}_{kj} \geq 0 \quad (7)$$

And

$$u_{ki} = \begin{cases} \bar{u}_{ki} + 1 - \sum_{i=1}^{c} \bar{u}_{ki} & (i = \arg min_l \, d_{kl}) \\ \bar{u}_{ki} & (otherwise) \end{cases} \quad (8)$$

In [24], Yasunori et al. constructed an algorithm of semisupervised standard fuzzy *c*-means clustering (SSFCM) by introducing supervised membership grade $\bar{u}_{ki}$into standard fuzzy *c*means clustering.

Algorithm 1 (SSFCM):

Step 1 Give supervised membership grades $\bar{U}$and set the initial values of *V*.

Step 2 Calculate *U* on fixing *V* by (5) (*m* >1) or (8) (*m* = 1).

Step 3 Calculate *V* on fixing *U* by (4).

Step 4 If the stop criterion satisfies, the algorithm is finished. Otherwise, go back to Step 2.

2.2 Proposed Method

From section 2.1, in order to develop an unmixing algorithm based on SSFCM, the supervised membership grades $\bar{U}$and set the initial values of *V* must be computed first. The endmember extraction algorithm VCA is applied to get k pixels that were chosen to be the purest where k is the suggested number of endmember and the estimated mixing matrix A.

From the pure pixels' indices, $\bar{U}$ is calculated by setting 1 in the matrix cell where the row represents the pixel number and the column represents the endmember fraction in the pixel. All $\bar{U}$ is zero elements except for these k cells turned to 1.

Also, V can be assigned to be equal the estimated mixing matrix A.

Now, the main aim of the new unmixing algorithm is to find *U* that minimizes the clustering error and from this final matrix *U*, the abundance matrices of endmembers can be extracted easily as the values in *U*represent the degree of membership (fraction or abundance) of each material (endmember)in a given pixel

Algorithm 2 (SSSFC):

Step 1 Apply VCA for k endmembers

Step 2 Get supervised membership grades $\bar{U}$and set the initial values of *V*.

Step 3 Calculate *U* on fixing *V* by (5) (*m* >1) or (8) (*m* = 1).

Step 4 Calculate *V* on fixing *U* by (4).

Step 5 If the stop criterion satisfies, the algorithm is finished. Otherwise, go back to Step 2.
Step 6 Abundance Maps = final *U*

The new unmixing model gives the abundance maps in a direct way from the membership grades without additional coefficients and parameters. It is not unsupervised (blind) model but it makes use from the priori knowledge one can get from the endmember extraction algorithms such as VCA, N-Finder, etc… The non-blindness of the model, given by a strong initialization, certainly improves the accuracy of the results.

3. Experimental Results

3.1Data Used

For experiments and evaluation of our new unmixing algorithm, two benchmark data are used. The first is the real data of Jasper Ridge [25] and the second is the synthetic data "Legendre"[26]. Jasper Ridge is a real popular hyperspectral data composed of 512 x 614 pixels. Each pixel is acquired at 224 channels starting from 380 nm to 2500 nm. The spectral resolution is up to 9.46 nm. A subimage of 100 x 100 pixels are considered and only 198 channels remained after removal due to dense water vapor and atmospheric effects. There are four endmembers latent in this data: road, soil, water and tree.

The Legendre synthetic images [26] have been generated using five selected endmembers from the USGS spectral library. Each image's spatial dimensions are of 128x128 pixels and they have 431 spectral bands. One of these images files corresponds to the free of noise hyperspectral synthetic image, and in the other four additive noise has been added to the synthetic image given a Signal to Noise Ratio (SNR) of 20, 40, 60 and 80db. The non linearity of this synthetic dataset was performed by the Fan unmixing model [27]

3.2 Quality Metrics

For a single estimated endmember, the spectral angle mapper (SAM) measures the similarity between the true endmember m and the estimated endmember $\tilde{m}$ as follows

$$SAM = arccos\left\langle \frac{m^T \tilde{m}}{\|m^T\| \quad \|\tilde{m}\|} \right\rangle \quad (9)$$

And the mean spectral angle mapper over all P endmembers is as follows

$$mSAM = \frac{1}{P}\sum_{p=1}^{P} SAM \quad (10)$$

For a single estimated abundance matrix, the root mean square error (RMSE) evaluates the error between the true abundance matrix a and the estimated abundance matrix $\tilde{a}$ and it is calculated as follows

$$RMSE = \sqrt{\frac{1}{NP}\sum_{n=1}^{N}\sum_{p=1}^{P}(a_{np} - \tilde{a}_{np})^2} \quad (11)$$

where$N$ is the total number of pixels and the mean RMSE over all abundance matrices is computed as

$$mRMSE = \frac{1}{P}\sum_{p=1}^{P} RMSE \quad (12)$$

Generally, small values of SAM and RMSE indicate a good accuracy

3.3 Results and Discussion

In this section, the results of applying the new algorithm (SSSFC) on two images are presented. The first image is the real data of Jasper Ridge and the second is the synthetic data of Legendre for different signal to noise (SNR) values such as SNR = 0, 20, 40, 60, and 80. We compare our results with those of four algorithms well known in the state-of-the art. Those algorithms used for comparison are the non-negative matrix factorization (NMF) [28], the sparsity-regularized NMF (SNMF)[29], the Simplex Projection Unmixing (SPU) [30], Different Metrics unmixing chain (DMaxD) [31].

Tables1 and 2 show the results in terms of Msam and Mrmse for the new algorithm and the four state-of-the art algorithms used in this paper.

In case of Jasper Ridge image, the SSSFC outperforms the others when considering the mean values over the four abundance maps. However, the SPU performs better than the SSSFC in case of the Legendre image with different SNRs. The SSSFC appears just after the SPU with slight differences in case of the Legendre image. Also, according to Figure 14, the SSSFC succeeded in getting three abundance maps (1, 4 and 5) accurately comparing with the ground truth images while the two others (2,

Table 1. The Values of MSAM and MRMSE for Jasper Ridge

	Jasper Ridge	
	Msam	Mrmse
SSSFC	**0.3526**	**0.5794**
NMF	0.4961	0.8330
SNMF	0.3862	0.7529
SPU	0.5343	0.8616
DMaxD	0.4081	0.8254

	Legendre									
	SNR = 0		**SNR = 20**		**SNR = 40**		**SNR = 60**		**SNR = 80**	
	Msam	Mrmse	Msam	Mrmse	Msam	Mrmse	Msam	Mrmse	Msam	Mrmse
SSSFC	0.1952	2.1959	**0.0759**	1.9376	0.1950	2.1726	0.1996	2.1914	0.1952	2.196
NMF	0.3203	2.6598	0.2804	3.6616	0.3356	1.9587	0.2786	4.1376	0.1946	2.3158
SNMF	0.2976	2.9597	0.298	2.9256	0.2977	2.9609	0.2977	2.9597	0.2976	2.9597
SPU	**0.0379**	**0.1765**	0.1612	**0.4462**	**0.1577**	**0.4205**	**0.1596**	**0.4199**	**0.1596**	**0.4177**
DMaxD	0.2871	1.3879	0.3545	1.4203	0.2023	1.4251	0.3332	1.6082	0.2991	1.9974

3) have very few different details.

Figures from 1to 12 show the different SAM and RMSE for each of the images and for in drawing the abundance maps compared by the other algorithms in most cases. each of the end members. It is clearly seen that the new algorithm had decreased the error

Table 2. The Values of MSAM and MRMSE for Legendre of different SNR values

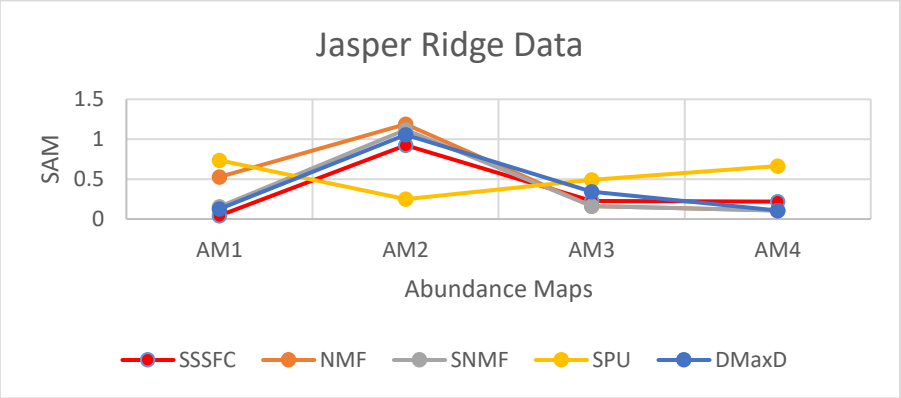

Figure 1. The SAM results of the four abundance maps of Jasper Ridge image

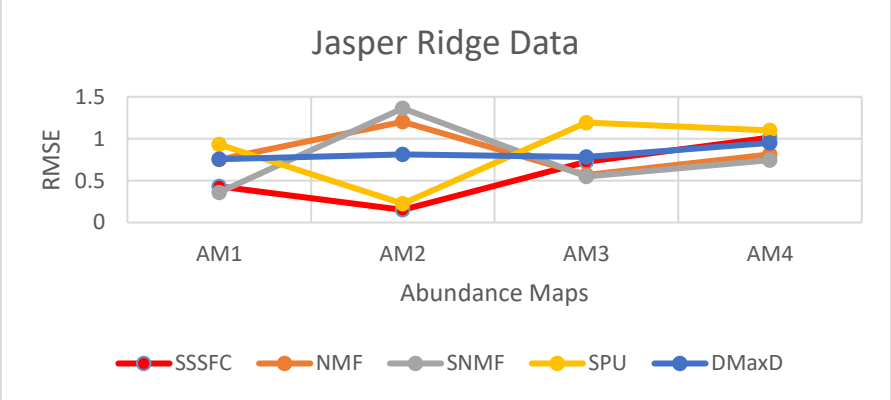

Figure 2. The RMSE results of the four abundance maps of Jasper Ridge image

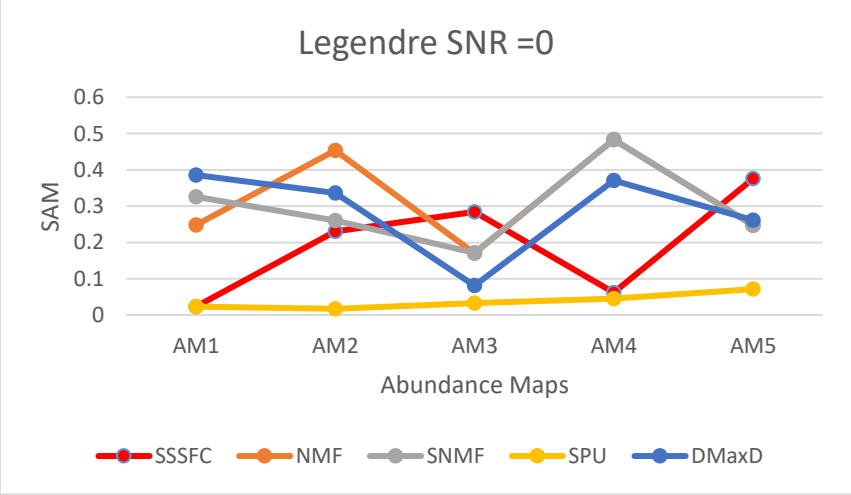

Figure 3. The SAM results of the five abundance maps of Legendre image SNR=0

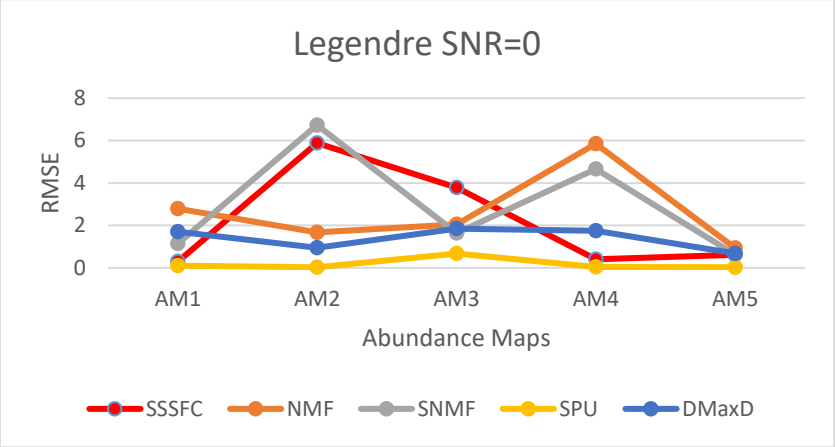

Figure 4. The RMSE results of the five abundance maps of Legendre image SNR=0

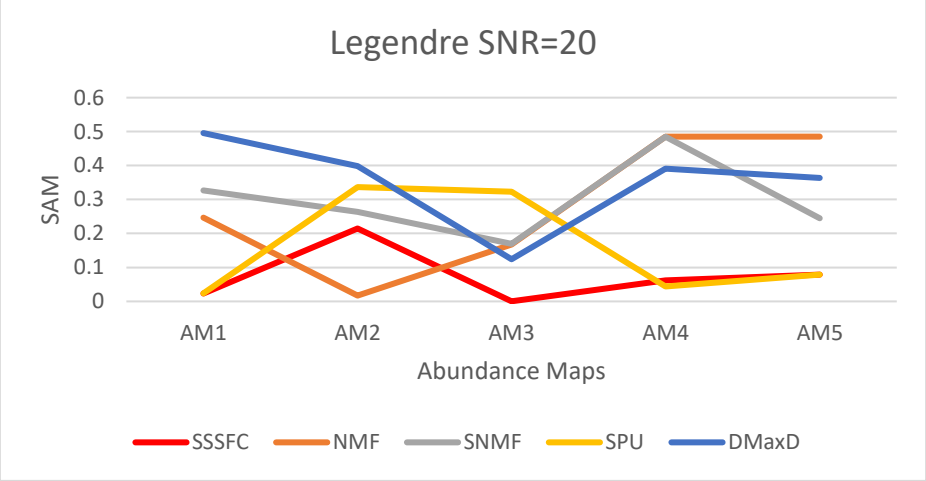

Figure 5. The SAM results of the five abundance maps of Legendre image SNR=20

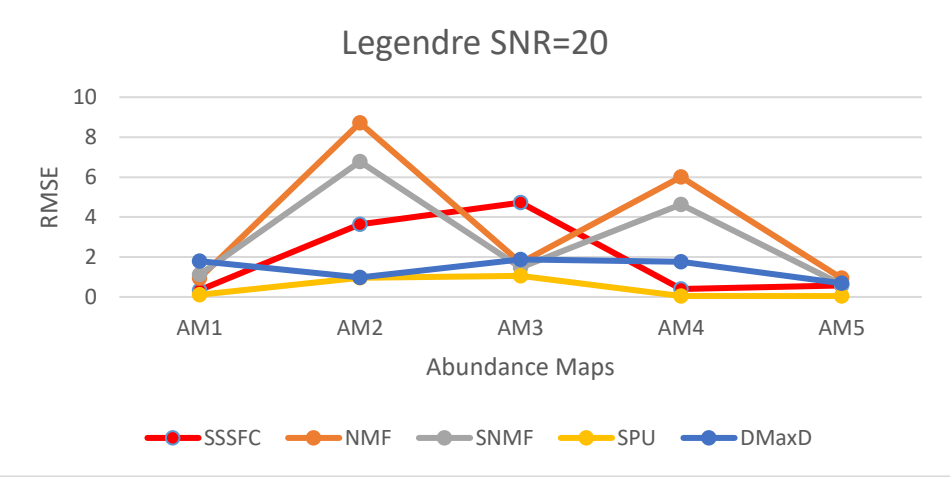

Figure 6. The RMSE results of the five abundance maps of Legendre image SNR=20

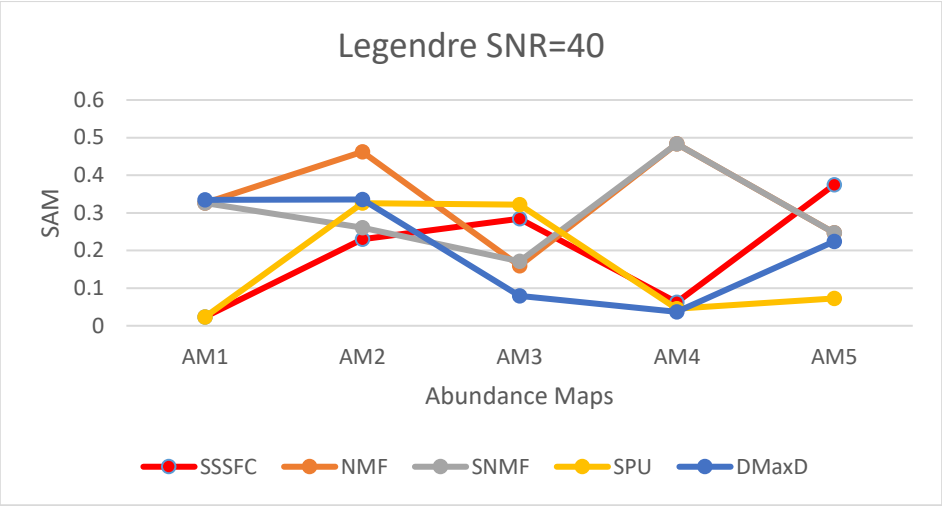

Figure 7. The SAM results of the five abundance maps of Legendre image SNR=40

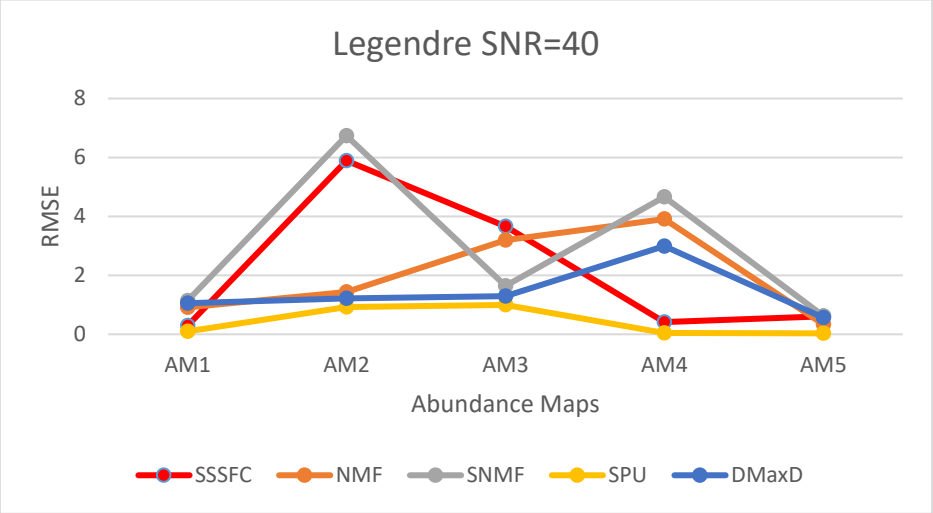

Figure 8. The RMSE results of the five abundance maps of Legendre image SNR=40

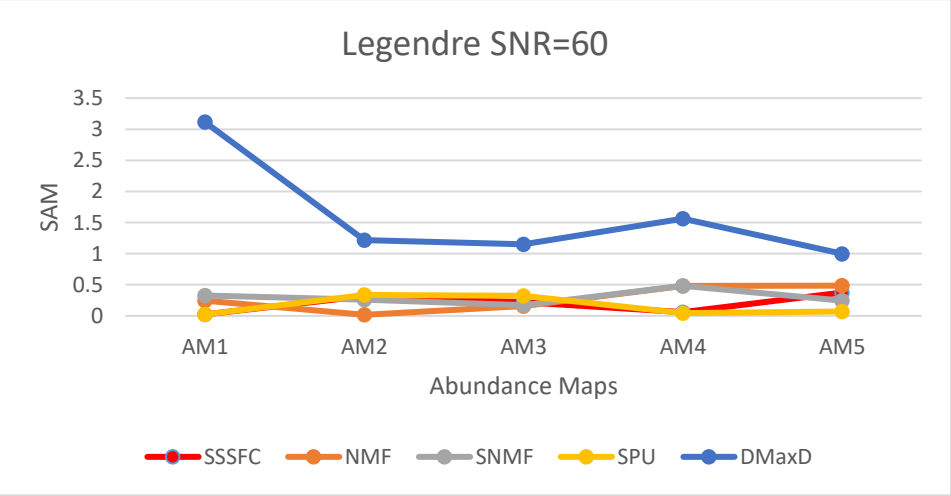

Figure 9. The SAM results of the five abundance maps of Legendre image SNR=60

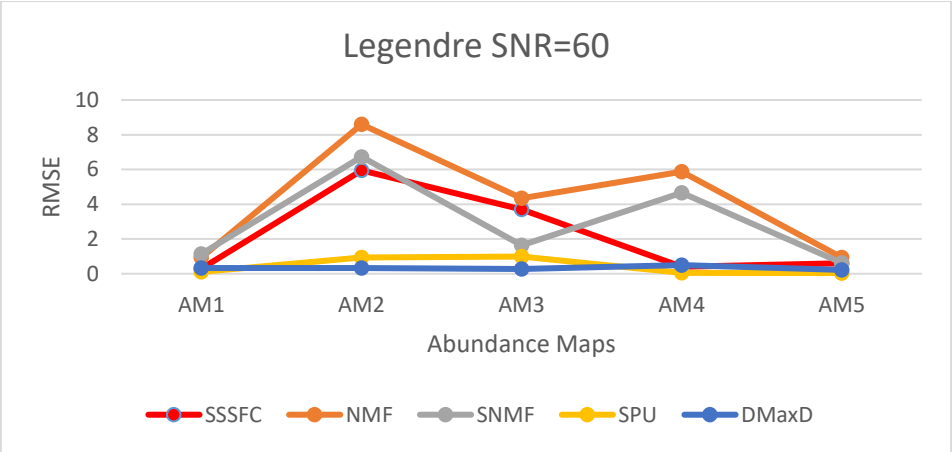

Figure 10. The RMSE results of the five abundance maps of Legendre image SNR=60

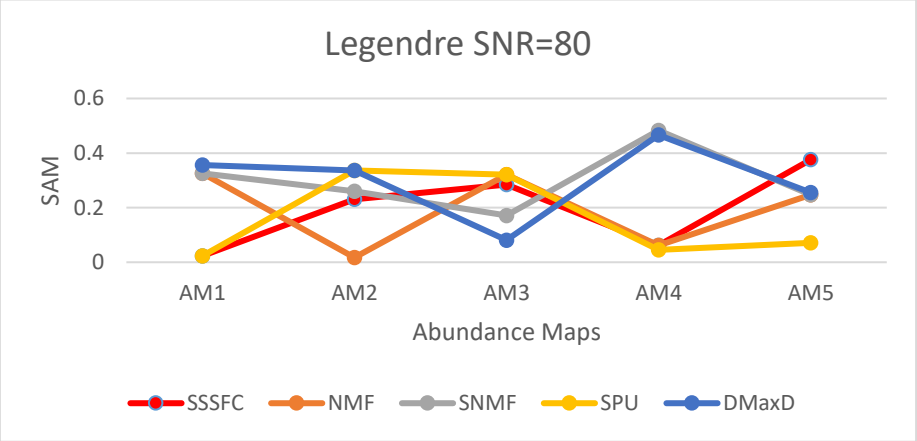

Figure 11. The SAM results of the five abundance maps of Legendre image SNR=80

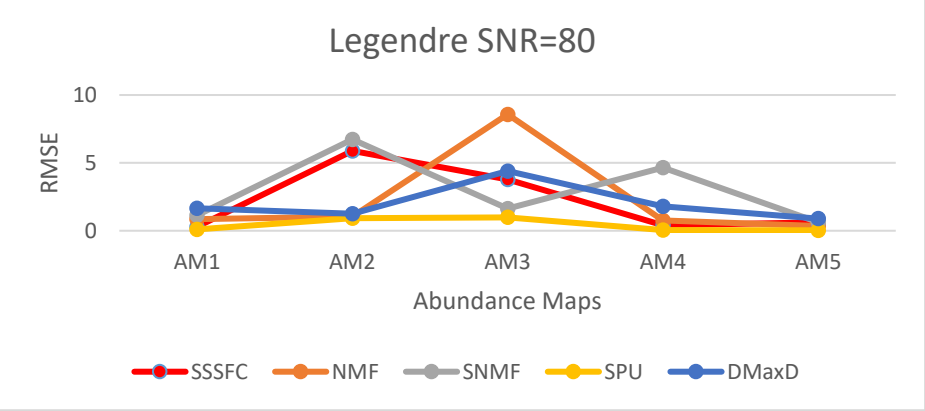

Figure 12. The RMSE results of the five abundance maps of Legendre image SNR=80

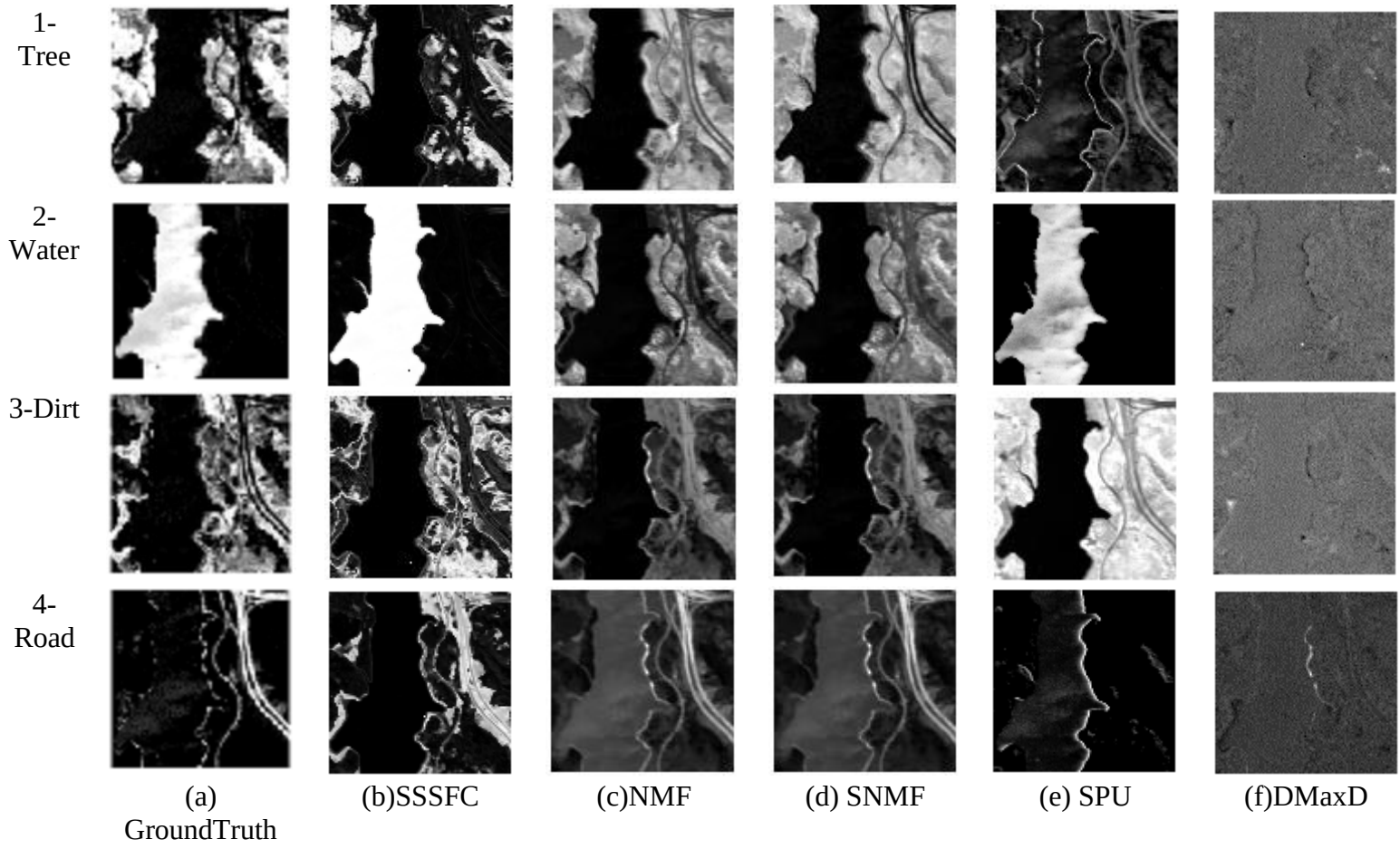

Figure 13. The abundance maps of Jasper Ridge image

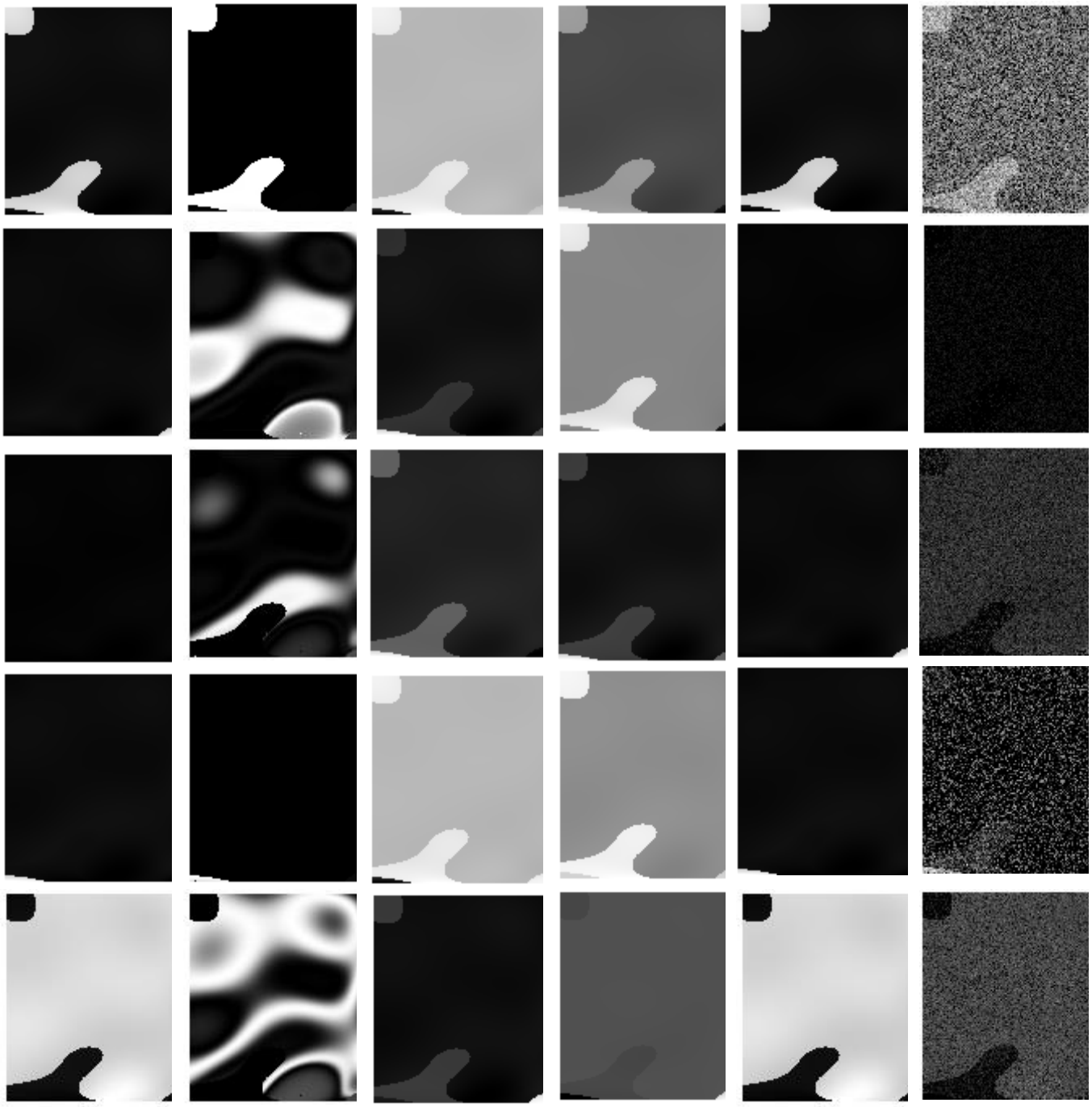

(a) GroundTruth (b)SSSFC (c)NMF (d) SNMF (e) SPU (f)DMaxD

Figure 14. The abundance maps of the Legendre image at SNR=0

4 Conclusions and Future Work

A new nonlinear spectral unmixing algorithm was presented in this paper. The new algorithm is based on the Fuzzy Semi Supervised Standard Clustering to conduct the abundance maps. Some pixels are labelled as pure initially using the Vertex Component Analysis algorithm and the rest of pixels are not labelled. Hence, the membership of the semi supervised fuzzy clustering can be initialized by those known pure pixels which

can get 1 for their corresponding endmember and 0 for the other endmembers. The new algorithm can easily conduct the new membership matrix after a number of iterations. This matrix equals the matrix of abundance maps. The new algorithm showsgood accuracy and efficiency when compared to four of the well-known state-of-the art algorithms.

As future work, it is suggested to extend the use of fuzzy logic in this area. New unmixing algorithms can be based on different types of fuzzy clustering.

Funding

Not applicable.

Conflict of interest/Competing interests

The author declare that they have no competing interests.

Availability of data and materials

Data is available by request to the author.

Authors' contributions

Shaheera designed the study, implemented the method, performed the experiments, conducted the results and wrote the manuscript.

References

[1] N. Dobigeon, J.-Y. Tourneret, C. Richard, J. C. M. Bermudez, S. McLaughlin, and A. O. Hero, "Nonlinear unmixing of hyperspectral images: Models and algorithms," IEEE Signal Process. Mag., vol. 31, no. 1, pp. 82–94, Jan. 2014.

[2] T. W. Ray and B. C. Murray, "Nonlinear spectral mixing in desert vegetation," Remote Sens. Environ., vol. 55, no. 1, pp. 59–64, Jan. 1996.

[3] R. Heylen, M. Parente, and P. Gader, "A review of nonlinear hyperspectral unmixing methods," IEEE J. Sel. Topics Appl. Earth Observ. Remote Sens., vol. 7, no. 6, pp. 1844–1868, Jun. 2014

[4] Dunn JC (1973) A fuzzy relative of the ISODATA process and its use in detecting compact well-separated clusters. J Cybern 3(3):32–57

[5] Venkateswarlu NB, Raju PSVSK (1992) Fast ISODATA clustering algorithms. Pattern Recogn 25(3):335–342

[6] Celik T (2009) Unsupervised change detection in satellite images using principal component analysis and K-means clustering. IEEE Geosci Remote SensLett 6(4):772–776

[7] Xu K, Yang W, Liu G (2013) Unsupervised satellite image classification using Markov field topic model. IEEE Geosci Remote SensLett 10(1):130–134

[8] Ahmed MN, Yamany SM, Mohamed N, Farag AA, Moriarty T (2002) A Modified fuzzy C-means algorithm for bias field estimation and segmentation of MRI data. IEEE Trans Med Imaging 21(3):193–199

[9] Cai W, Chen S, Zhang D (2007) Fast and robust fuzzy C-means clustering algorithms incorporating local information for image segmentation. Pattern Recogn 40(3):825–838

[10] Krinidis S, Chatzis V (2010) A robust fuzzy local information C-means clustering algorithm. IEEE Trans Image Process 19(5):1328–1337

[11] Li N, Huo H, Zhao Y (2013) A spatial clustering method with edge weighting for image segmentation. IEEE Geosci Remote SensLett 10(5):1124–1128

[12] Bezdek JC (1981) Pattern recognition with fuzzy objective function algorithms. Plenum, New York

[13] Chuang KS, Tzeng HL, Chen S, Wu J, Chen TJ (2006) Fuzzy c-means

clustering with spatial information for image segmentation. Comput Med Imaging Graph 30(1):9–15

[14] Shang R, Tian P, Jiao L, Stolkin R, Feng J, Hou B, Zhang X (2016) A spatial fuzzy clustering algorithm with kernel matrix based on immune clone for SAR image segmentation. IEEE J Sel Top Appl Earth Observ Remote Sens 9(4):1640–1652

[15] Zhao Q, Li X, Li Y, Zhao X (2017) A fuzzy clustering image segmentation algorithm based on hidden markov random fiel models and voronoi tessellation. Pattern RecognLett 85(1):49–55

[16] Kahali S, Sing JK, Saha PK (2019) A new entropy-based approach for fuzzy cmeans clustering and its application to brain MR image segmentation. Soft Comput 23:10407–10414

[17] Das, S. and Chakravortty, S., 2021. Efficient entropy-based spatial fuzzy c-means method for spectral unmixing of hyperspectral image. *Soft Computing*, pp.1-19.

[18]Zare, A., 2011, July. Spatial-spectral unmixing using fuzzy local information. In *2011 IEEE International Geoscience and Remote Sensing Symposium* (pp. 1139-1142). IEEE.

[19]Silván-Cárdenas, J.L. and Wang, L., 2010. Fully constrained linear spectral unmixing: Analytic solution using fuzzy sets. *IEEE Transactions on Geoscience and Remote Sensing*, *48*(11), pp.3992-4002.

[20]Bastin, L., 1997. Comparison of fuzzy c-means classification, linear mixture modelling and MLC probabilities as tools for unmixing coarse pixels. *International Journal of Remote Sensing*, *18*(17), pp.3629-3648.

[21]Zare, A. and Gader, P., 2011, June. Piece-wise convex spatial-spectral unmixing of hyperspectral imagery using possibilistic and fuzzy clustering. In *2011 IEEE International Conference on Fuzzy Systems (FUZZ-IEEE 2011)* (pp. 741-746). IEEE.

[22] Chaudhry, F., Wu, C.C., Liu, W., Chang, C.I. and Plaza, A., 2006. Pixel purity index-based algorithms for endmember extraction from hyperspectral imagery. *Recent advances in hyperspectral signal and image processing*, *37*(2), pp.29-62.

[23]Nascimento, J.M. and Dias, J.M., 2005. Vertex component analysis: A fast algorithm to unmix hyperspectral data. *IEEE transactions on Geoscience and Remote Sensing*, *43*(4), pp.898-910.

[24] Yasunori, E., Yukihiro, H., Makito, Y. and Sadaaki, M., 2009, August. On semi-supervised fuzzy c-means clustering. In 2009 IEEE International Conference on Fuzzy Systems (pp. 1119-1124). IEEE.

[25] Hyperspectral real dataset (http://lesun.weebly.com/hyperspectral-data-set.html) last accessed 8 March 2021

[26] Hyperspectral synthetic dataset (http://www.ehu.eus/ccwintco/index.php/Hyperspectral_Imagery_Synthesis_tools_for_MATLAB): last accessed 7 March 2021

[27]W. Fan, B. Hu, J. Miller, and M. Li, "Comparative study between a new nonlinear model and common linear model for analysing laboratory simulated forest hyperspectral data," Int. J. remote sens., vol. 30, no. 11, pp. 2951–2962, 2009.

[28] Parente, M., Zymnis, A., Skaf, J. and Bishop, J., 2006, October. Spectral unmixing with nonnegative matrix factorization. In *Remote Sensing for Environmental Monitoring, GIS Applications, and Geology VI* (Vol. 6366, p. 63660B). International Society for Optics and Photonics.

[29] He, W., Zhang, H. and Zhang, L., 2016. Sparsity-regularized robust non-negative matrix factorization for hyperspectral unmixing. *IEEE Journal of Selected Topics in Applied Earth Observations and Remote Sensing*, *9*(9), pp.4267-4279.

[30] R. Heylen and D. Burazerovic and P. Scheunders. "Fully Constrained Least Squares Spectral Unmixing by Simplex Projection," *IEEE Trans. Geosci. Remote Sens.*, vol. 49, no. 11, pp. 4112-4122, Nov. 2011

[31] Heylen, R., Scheunders, P., Rangarajan, A. and Gader, P., 2014. Nonlinear unmixing by using different metrics in a linear unmixing chain. *IEEE Journal of Selected Topics in Applied Earth Observations and Remote Sensing*, 8(6), pp.2655-2664.